

The High Inclination Solar Mission

Kobayashi, Ken¹, Johnson, Les¹, Thomas, Herbert D.¹, McIntosh, Scott²,
McKenzie, David¹, Newmark, Jeffrey³, Heaton, Andy¹, Carr, John¹,
Baysinger, Mike¹, Bean, Quincy¹, Fabisinski, Leo¹, Capizzo, Pete¹,
Clements, Keith¹, Sutherlin, Steve¹, Garcia, Jay¹, Medina, Kamron⁴, and
Turse, Dana⁴

¹NASA Marshall Space Flight Center

²High Altitude Observatory

³NASA Goddard Space Flight Center

⁴Roccor, LLC

June 8, 2020

Abstract

The High Inclination Solar Mission (HISM) is a concept for an out-of-the-ecliptic mission for observing the Sun and the heliosphere. The mission profile is largely based on the Solar Polar Imager concept[Liewer et al., 2008]; initially taking ~ 2.6 yrs to spiral in to a 0.48 AU ecliptic orbit, then increasing the orbital inclination at a rate of ~ 10 degrees per year, ultimately reaching a heliographic inclination of >75 degrees. The orbital profile is achieved using solar sails derived from the technology currently being developed for the Solar Cruiser mission, currently under development.

HISM remote sensing instruments comprise an imaging spectropolarimeter (Doppler imager / magnetograph) and a visible light coronagraph. The in-situ instruments include a Faraday cup, an ion composition spectrometer, and magnetometers. Plasma wave measurements are made with electrical antennas and high speed magnetometers.

The $7,000\text{ m}^2$ sail used in the mission assessment is a direct extension of the 4-quadrant $1,666\text{ m}^2$ Solar Cruiser design and employs the same type of high strength composite boom, deployment mechanism, and membrane technology. The sail system modelled is spun (1 rpm) to assure required boom characteristics with margin. The spacecraft bus features a fine-pointing 3-axis stabilized instrument platform that allows full science observations as soon as the spacecraft reaches a solar distance of 0.48 AU.

1 Introduction

The value of a high ecliptic inclination vantage point for solar and heliospheric observations has long been recognized. To date, the only mission that provided a vantage point from

outside the ecliptic plane was the Ulysses mission [Wenzel et al., 1992]. However, Ulysses’ payload was limited to in-situ instruments, and because of the long period orbits necessitated by the Jupiter gravity assist, it only made 3 orbits (3 passes above north and south poles of the Sun respectively).

Apart from Ulysses, the only spacecraft with non-negligible orbital inclination is the recently launched Solar Orbiter [Marsch et al., 2005], which will reach a heliographic inclination of 24 degrees at the end of the 7-year mission, and 33 degrees with an additional three years of extended mission. However, even the 33 degree heliographic inclination is marginal for observing the high latitude structures through helioseismology, and inadequate for observing the solar wind from polar regions.

Several concepts have been put forward for out-of-the-ecliptic missions, some using solar sails. The Solar Polar Imager [Liewer et al., 2008] (SPI) or the POLARIS [Appourchaux et al., 2009] concept proposed a solar sail mission with a 28,800 m² sail and 325 kg payload, achieving a final orbit of 0.48 AU and 75 degree inclination. SPI is specifically endorsed by the 2013 Decadal Strategy for Solar and Space Physics (Heliophysics) National Research Council [2013]. Other proposals include The POLAR investigation of the Sun —POLARIS [Appourchaux et al., 2009] and Solar Polar Diamond Explorer (SPDEx) [Vourlidas et al., 2018]. But these concepts require significant technological development.

Since the original SPI concept was originally formulated, there has been significant development and testing in solar sail technology. Japan Aerospace Exploration Agency (JAXA) successfully deployed the IKAROS solar sail technology [Yamaguchi et al., 2010], and The Planetary Society also demonstrated successful deployment of solar sails [Ridenoure et al., 2015]. Marshall Space Flight Center (MSFC) and the Jet Propulsion Laboratory (JPL) have developed the NEA Scout [Russell-Lockett et al., 2020], currently scheduled for launch in 2021. Solar Cruiser is currently in phase-A study at MSFC, and uses a 16,000 m² sail based on the 82 m² NEA Scout sail design.

The High Inclination Solar Mission (HISM) is a concept study conducted at the MSFC Advanced Concepts Office (ACO), with the goal of extending the Solar Cruiser sail design to build a solar and heliospheric mission.

2 Science Rationale

A high latitude imaging system - like HISM - offers an opportunity to routinely observe the Sun’s polar regions. From that unique vantage point a broad spectrum of scientific challenges can be addressed, from studies of the Sun’s internal circulation and convection, detailed measurements of the fast solar (polar) wind and its interface with that from the magnetically closed equatorial regions. Beyond that, a polar vantage point permits the first synchronic study in the development of longitudinal waves that form on the Sun’s activity belts that shape space weather and give rise to the largest solar eruptions.

The polar regions present tantalizing observational hints of the Sun’s cyclic behavior, and possibly that they play a critical role in establishing that critical behavior. Consider the composite of solar filament progression over the last 140 years constructed from a number of observatories [McIntosh et al., 2019, and Fig. 1]. Paying attention to the position and timing of the highest latitude filaments in the system we notice that McIntosh et al. [2019] spend

much of their time around 55 degrees latitude, only progressing poleward on one occasion per solar cycle - at the start of the polar magnetic field reversal. This latitude is also the lowest of polar coronal holes [McIntosh et al., 2014] and thus appears to present a robust canonical boundary between the polar and equatorial environments. *What is so special about 55 degrees?*

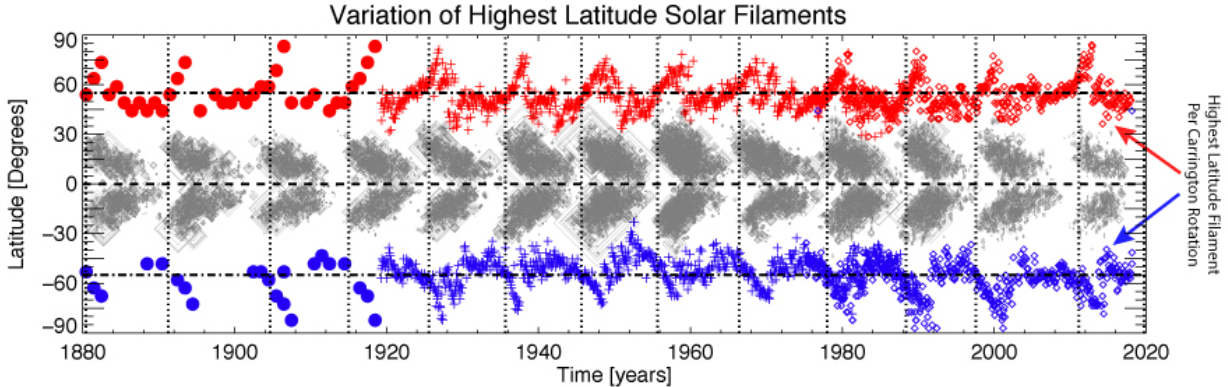


Figure 1: The 140 year record of solar filaments as observed in $H\alpha$ observations from three sites: Arcetri Astrophysical Observatory (AO; 1880–1929), Meudon Observatory (MO; 1919–1989), and the Kislovodsk Observatory (KO; 1980–2018). Contrast the sunspot butterfly pattern in gray with the modulation of the highest latitude filaments present at each timestep (red:north; blue:south) and each observatory. In each figure we show the locations of the terminators as provided by McIntosh et al. [2014] as vertical dotted lines (see above). The dot-dashed lines at 55° in each hemisphere are added for reference.

The vertical dashed lines in Fig. 1 represent the termination points of the magnetic activity bands that belong to the 22-year Hale magnetic cycle at the Sun's equator [McIntosh et al., 2019]. At those times, not only does the polar reversal process (REF) start, but we observe the birth of the sunspot cycle at mid-solar latitudes. Emphasizing the cyclic nature and importance of 55 degrees, we can construct a superposed epoch analysis (SEA) using the Hale cycle terminations as the key time. Figure 2 contrasts the SEA of 140 years of the filament density on the solar disk with the sunspot record over the same timeframe. That analysis shows that the sunspot progression is a subset of the Hale cycle manifestation that has its start at around 55 degrees around 10 years before. *Does this mean that the Sun's dynamo process originates at 55 degrees and is more cyclic than the sunspot modulation would lead us to believe?*

The results shown above illustrate that imaging of the Sun's high latitudes is possible when line-of-sight measurements become limited, they have been made possible by the cataloging of prominent features on the disk and above the limb. However, to probe and understand the physical processes taking place at 55 degrees that give rise to these features requires a study of the circulatory and convective flows and a high latitude observing platform.

Helioseismic measurements have probed the nature of the Sun's interior and rotational characteristics for several decades. Ground-breaking inversions of line-of-sight Doppler measurements from the ecliptic have revealed an internal rotational structure that appears to be rigid below 70 percent of the Sun's radius, but highly structured with depth in the outer

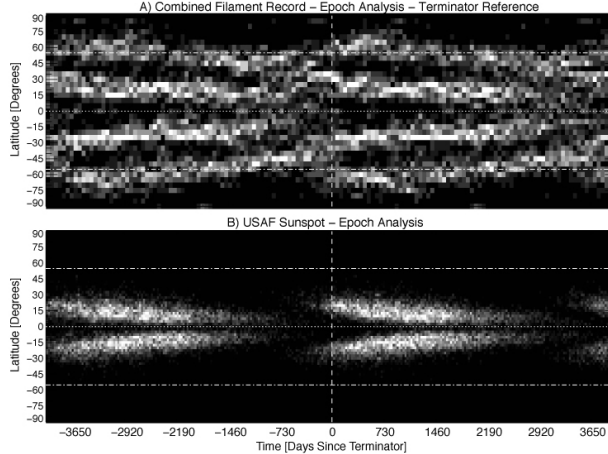


Figure 2: Comparing the SEA-derived mean patterns of filaments, and sunspots from 140 years of observations. The vertical dashed line indicates a time of zero. The horizontal dashed line indicates the equator while the horizontal dot-dashed lines signify 55° latitude in each hemisphere.

30% [Thompson et al., 1996]. The left panel of Fig. 4 shows the state of the art in understanding the Sun's internal rotation that, when presented in a slightly different format (right panel) shows that the inferred rotational profile with depth is uniform around 55° for a considerable depth (0.8 - 0.95 solar radii), hinting at the presence of a significant shear in the plasma flow there (possibly even an interface between the polar and equatorial regions). Analogous helioseismic investigations over the same epoch [e.g., Howard and Labonte, 1980, Howe et al., 2000] have revealed the presence of a banded flow pattern - of alternating fast and slow regions - that mirror the Hale magnetic cycle pattern deduced from surface features [e.g., Snodgrass and Wilson, 1987, Wilson et al., 1988, McIntosh et al., 2014].

From the particulate perspective of the solar wind the long periods of time where polar coronal holes are visible provide two unique scientific opportunities for a high-latitude platform: 1) the combined imaging and in-situ study of fast solar wind direct from its origin as inferred from Ulysses and SoHO [e.g., Hassler et al., 1999, McComas et al., 2000, McIntosh et al., 2011], including the ubiquitous Alfvénic and magneto-convective energy input [e.g., de Pontieu et al., 2007, De Pontieu et al., 2007, Tomczyk et al., 2007, McIntosh, 2012], and 2) in the transitions from the polar crown to the polar coronal hole environment we would sample the interface region between open and closed magnetic field to look for the signatures of interchange magnetic reconnection observed by Parker Solar Probe [Fisk et al., 1999, Fisk and Kasper, 2020].

The epoch from 2010 to 2014 created a unique opportunity in the space era - for the first time we had complete coverage of the solar disk in (extreme ultraviolet - EUV) observations provided by SOHO, SDO and the twin STEREO spacecraft. This unique set of observations permitted the study of the Sun's longitudinal behavior and to take a meteorological approach to the analysis of our star's atmosphere (see Fig. 5). It was identified that certain longitudes remained active over many rotations, with those regions persistently producing a host of strongly eruptive behavior [e.g., McIntosh et al., 2015]. Further, in studying the behavior of

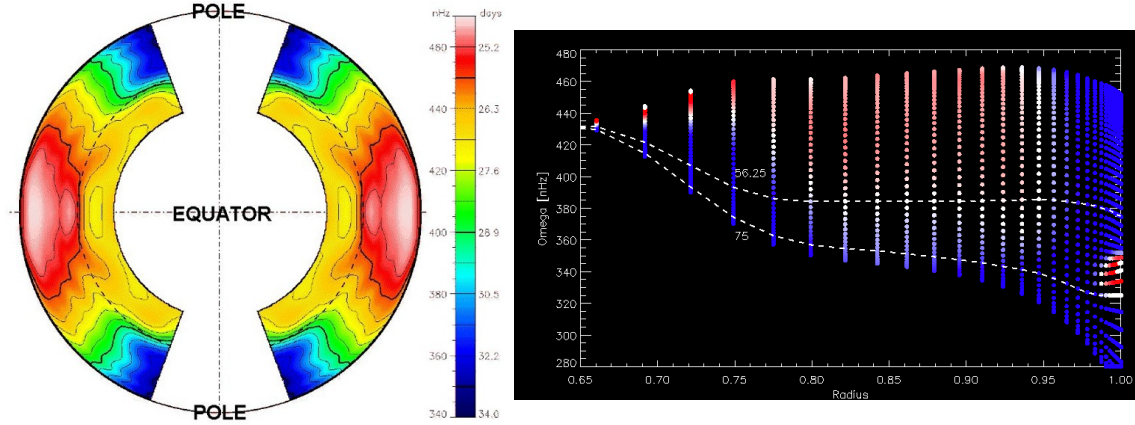


Figure 3: Left: The rotation rate inside the Sun, determined by helioseismology using instruments aboard the showing the location of the tachocline where rigid rotation in the radiative zone gives way to differential rotation in the convective zone Thompson et al. [1996]; Right: Higher spatial resolution version of rotation profile showing the average rotation profile (symmetrised) over the whole of the SDO/HMI record. Notice that near 55 degrees - the variation of the rotation rate with depth is close to zero.

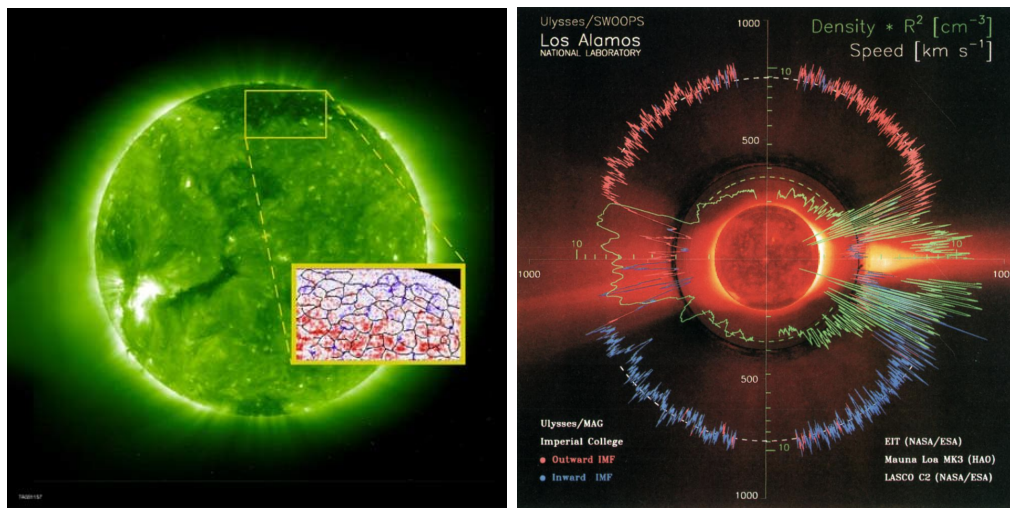


Figure 4: Left: The preferential plasma outflow visible in the ultraviolet spectral lines that form in the solar transition region at the supergranular network of polar coronal holes - the roots of the fast solar wind [Hassler et al., 1999]; Right: The measurements of Ulysses demonstrated the stark transition between the slow (magnetically closed) and fast (magnetically open) solar wind regimes [McComas et al., 2000].

small dipolar regions (EUV brightpoints) in the composite observations, it was discovered that the Sun's magnetic activity bands displayed the characteristic signature of (magnetized) Rossby waves [McIntosh et al., 2017] that drove the longitudinal behavior of magnetic flux emergence and hence the key ingredients of space weather. Subsequent effort invested in

understanding the nature of these waves [Dikpati and McIntosh, 2020] has demonstrated the potential of breakthrough by developing greater predictability of space weather phenomena and the magnetic activity in which it is rooted. A high latitude observing platform like HISM will have the opportunity to observe the development of these waves, their longitudinal structure and evolution and finally the organization of phenomena that they drive.

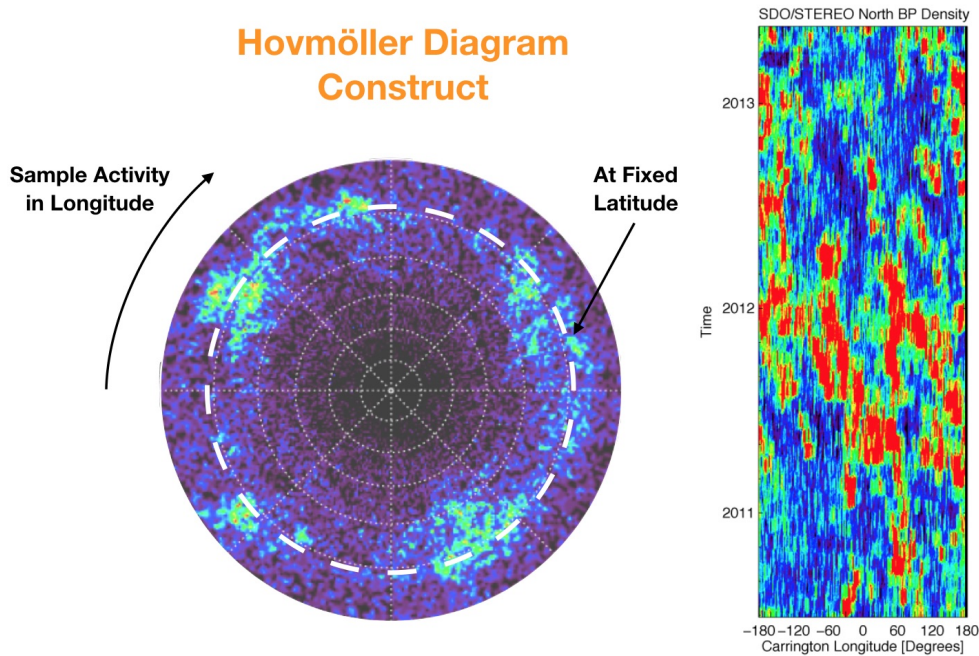


Figure 5: Illustrating the concept of a Hovmöller diagram. Left: For a synchronous spherical dataset a Hovmöller diagram is constructed by sampling the longitudinal evolution of the system in a narrow range of latitudes over time. Right: The annuli are then stacked to represent the passage of time. In the example shown the density of synchronous EUV BrightPoint density is shown and was the original example used to diagnose the presence of Rossby waves in the global-scale magnetic flux systems of solar interior.

2.1 Mission Science Objectives

Using the examples presented above in concert with previous investigations of high-latitude and polar observing platforms [Appourchaux et al., 2009, Alexander et al., 2005, Liewer et al., 2008, Liewer, 2013, Appourchaux et al., 2017, Berger et al., 2019] we formulate the following high level science goals for HISM that meet the those of the National Academy Decadal Survey “Solar and Space Physics: A Science for a Technological Society” [National Research Council, 2013].

1. Understand the Sun’s internal structure and surface dynamics in the polar regions
2. Understand the 3D structure of the Solar/heliospheric magnetic field and its variation over time

Table 1: Instrument specifications, traceability, and requirements imposed on the spacecraft. The "Science Goals" column indicates flowdown from the science objectives listed in Section 2.1.

Instrument	Doppler & Stokes Imager	Coronagraph	Magnetometers	Plasma Spectrometer	Faraday Cup	Electric Antennas	Search coil Magnetometer
Science Goals	1, 2, 5	2, 5	2, 5	2, 3, 5	2, 4, 5	2, 5	2, 5
Field of View	1.5°x1.5°	16°	N/A	360° azimuth × 70° elevation	cone with >30° half-angle	2 π	N/A
Pointing	0.5° of Sun center	<2' of Sun center	N/A	1 deg of Sun	1 deg of Sun	none	none
Pointing Knowledge	<20 arcsec	<20 arcsec	~0.1 deg	1 deg	< 0.5 deg	~1 deg	~1 deg
Pointing Stability	20" over 10 s	7" over 1 s	N/A	1 deg over 65 s	0.1 deg over 1 s		
Power	37 W	15 W	3 W	4 W	4 W	7 W	9 W
Data Volume	75 kbps	40 kbps	0.6 kbps	0.2 kbps	0.2 kbps	3 kbps	2 kbps
Mass (basic)	17 kg	10 kg	4 kg	2 kg	4 kg	6 kg	3 kg

3. Understand the variations in the solar wind speed and composition at high latitudes
4. Understand the origin and acceleration mechanism of solar energetic particles
5. Evaluate the use of high-latitude data for space weather predictions and warnings

3 Science Instruments

The instrument suite loosely based on the POLARIS study [Liewer et al., 2008], but descoped and updated where appropriate to meet the science objectives (Section 2.1 and achieve a feasible mission. Their specifications and traceability to the science goals are shown in Table 1.

3.1 Doppler and Stokes Imager (DSI)

The Doppler and Stokes Imager is used to measure the photospheric vector magnetic field structure near the Sun's poles and to probe the interior of the Sun, including its high latitude regions, through helioseismology. The instrument is an imaging spectropolarimeter consisting of a telescope, polarizer and a narrowband tunable filter. The instrument is based on the Heliospheric and Magnetic Imager (HMI) on the Solar Dynamics Observatory (SDO) satellite as well as the Polarimetric and Helioseismic Imager for Solar Orbiter (SO/PHI). The field of view will be adjusted to 1.5 x 1.5 degree, to allow full disk (1 deg diameter) observation at 0.48 AU distance from the Sun. The DSI mass is estimated as 15 kg total, based on preliminary instrument designs by partner organizations (Jeffery Newmark, private communications).

The instrument contains image stabilization system (tip/tilt mirror or similar) with a >20 arcsec stroke, but no roll correction. This imposes an instrument pointing requirement of 20 arcsec tip/tilt stability during exposure (up to 10s), and roll stability of also 20 arcsec over 10s, to insure <0.2 movement of the solar limb during exposure.

The data rate is based on the assumption of 45 second cadence for velocity images and 5 minute cadence for Stokes parameter images, and lossless compression factor of 2. Helioseismology observations require long periods (days to weeks) of contiguous observations, so the SPI is required to be continuously sun-pointing except for flip maneuvers when crossing the equator; any design that requires periodic re-pointing of the spacecraft for data downlink is not allowed.

3.2 White Light Coronagraph

The White Light Coronagraph is an externally occulted Lyot coronagraph, similar to the STEREO (Solar Terrestrial Relations Observatory) Sun Earth Connection Coronal and Heliospheric Investigation (SECCHI) COR2 and SOHO (Solar and Heliospheric Observatory) Large Angle and Spectrometric Coronagraph (LASCO) C2 instruments. The primary purpose is to observe CME brightness and linear polarization.

A coronagraph by its nature cannot have any optics in front of the occulter; the occulter and coronagraph aperture must be aligned to the Sun to minimize scattered light. Because the Doppler and Stokes Imager has a tip/tilt mirror, the coronagraph defines the overall pointing requirement for the Solar Polar Imagers bus, or its remote sensing instrument platform (instrument bus). The actual requirement is dependent on the occulter diameter (inner edge of the field of view), which has not yet been determined from the science goals. Following discussion with Joan Burkepile, for this study, the pointing accuracy requirement was defined as 2 arcminutes, similar to the STEREO SECCHI COR2. The SECCHI COR2 has an inner FOV of 2.5 R., i.e. $1.5 R. = 23$ between the solar limb and the inner FOV edge. At 0.48 AU, the same 23 margin translates to 0.75 R., resulting in an occulter diameter of 1.75 R.. The size and mass are consistent with Appourchaux et al.

3.3 Magnetometers

The magnetometer system is based on the Appourchaux study, with all specifications taken from that paper. The system consists of two laser-pumped vector helium magnetometers, mounted on a 5m boom, 1.5m apart.

The magnetometer boom design is assumed to be the ATK (now Northrop Grumman) CoilABLE mast, used as magnetometer booms on most interplanetary and earth-orbiting satellites. Ideally the magnetometer boom should carry nothing but the magnetometers; however, DSCOVR mounted the solar wind instruments on the same boom as the magnetometers. Based on this precedent, and due to the crowded space around the SPI bus (plasma antennas, communication antennas, sail, radiators and solar arrays), the solar wind instruments were allowed to be mounted to the same boom.

3.4 Faraday Cup

The Faraday Cup instrument is envisioned as a close copy of the Solar Probe Cup (SPC), part of the Solar Wind Electron Alphas Protons (SWEAP) suite on the Parker Solar Probe (PSP) spacecraft (Case et al., 2020). The PSP/SPC is sun-viewing during the encounter phase between 0.25 AU down to the eventual perihelion on 9.86 solar radii from the center of the Sun. As such, the PSP/SPC was designed to withstand a very intense solar radiation environment. For the HISM mission at 0.48 AU, some different material choices and reduced radiation shields could allow for a reduction in mass relative to the PSP application. A larger diameter of the limiting aperture could allow for the Faraday Cup to have a field of regard (FOR) of 45 degrees half-diameter and maintain a large dynamic range for flux. The energy range for solar wind ions would be about 100 eV to 6000 eV (corresponding to protons with speeds from 139 to 1072 km/s). Electrons with an energy/charge between 100 eV and 1500 eV can also be measured. The variable command, AC operation, and synchronous detection of the HISM/Faraday Cup would be the same as the PSP/SPC which allows 1-dimensional Velocity Distribution Functions obtained from one every 4 seconds to one every 250 ms. These time scales can be tailored to needs of the mission.

3.5 Plasma Spectrometer

The Plasma Spectrometer is assumed to be identical to the Fast Imaging Plasma Spectrometer (FIPS) on the MESSENGER spacecraft (Andrews et al., 2007), which traces its heritage to the Solar Wind Ion Composition Spectrometer (SWICS) instrument on the Advanced Composition Explorer (ACE). It consists of an electrostatic analyzer and time-of-flight telescope, and is sensitive to 0.2 – 10 keV/Q solar wind ions. It has a field of view (FOV) of 1.4 pi steradians, i.e. 60 degree half-diameter cone. A nominal energy scan occurs every 65 seconds with a burst mode of 2 seconds over a narrow energy range. Mass resolution is such that C, N, and O are well separated.

3.6 Radio and Plasma Wave Package

This package consists of two sets of sensors - a set of electrical monopole antennas and a search coil magnetometer and readout / data processing electronics. The electrical antennas are assumed to consist of 3 antennas, each 6m long and 1.4 kg in mass, based on the Solar Probe FIELDS antennas. These are deployed as far away from each other as possible, while maximizing separation from other deployable structures and the sail. The search coil magnetometer is assumed to mount on the magnetometer boom. The electronics package is 5kg.

3.7 Mission Requirements

The driving requirements & assumptions of the design are:

- Accommodate science instruments as shown in Table 1
- Dedicated launch to $C_3 = 0$ trajectory

- Spiral-in to 0.48 AU circular ecliptic orbit, followed by cranking to 75° inclination
- Utilize Solar Cruiser sail technology scaled up to 7000 m²
- Total mission life of 11 years
- Maximize science observing time

The HISM mission has been designed by the NASA MSFC Advanced Concepts Office (ACO) based on these requirements. Existing high-TRL components are used wherever possible.

4 Spacecraft Design

4.1 Overview

The HISM spacecraft consists of the Science Bus, Lower Bus, sail assembly, and the Spin-up Bus (Figures 6,7). The sail spins at ~ 1 rpm rate to allow centrifugal force to augment the stiffness (Section 4.4). Attached to the sail is the Spin-up Bus, which contains a propulsion system for attitude control prior to sail deployment and for initiating the sail spin during sail deployment. The Spin-up Bus is jettisoned after sail deployment; the rest of the spacecraft is hereafter referred to as the sailcraft. The Science Bus is a fine-pointing platform containing all science instruments and their electronics, as well as the solar panels. The Lower Bus contains the remaining avionics subsystems, and while it is de-spun (decoupled from the rotating sail through a de-rotation mechanism), it is not required to meet the fine pointing requirements of the science instruments.

The mass of the sailcraft is estimated at 240 kg, or 293 kg including margin (mass growth allowance consistent with AIAA S-120A-2015). This results in sailcraft characteristic acceleration of $A_c = 0.265$ mm/s² or $A_c = 0.217$ mm/s² respectively. The total launch mass is 358 kg including margin.

4.2 Sailcraft Bus

The spinning solar sail is a major design constraint, as a spinning platform is unsuitable for remote sensing observations. One possible solution is to start science observations only after the sailcraft has reached the target high-inclination orbit and the sail has been jettisoned. Alternatively, a de-spin mechanism in the sailcraft can allow full science operations while the sail is still attached and spinning. The latter approach was chosen for HISM to maximize science returns by starting observations early in the mission and continuing these observations from different orbital inclinations. This also allows the sailcraft to rely on Reflectivity Control Devices (RCDs) for momentum management, eliminating the need for any propulsion system on the sailcraft for desaturating the momentum wheels.

Further, a large deployable structure such as a solar sail cannot be assumed to be perfectly symmetric, and asymmetries may lead to precession of the sail. Therefore the HISM bus design consists of 2 sections: the fine-pointing Science Bus and the Lower Bus, as shown in Figures 6 and 8. The Lower Bus is de-spun from the spinning sail through a motorized

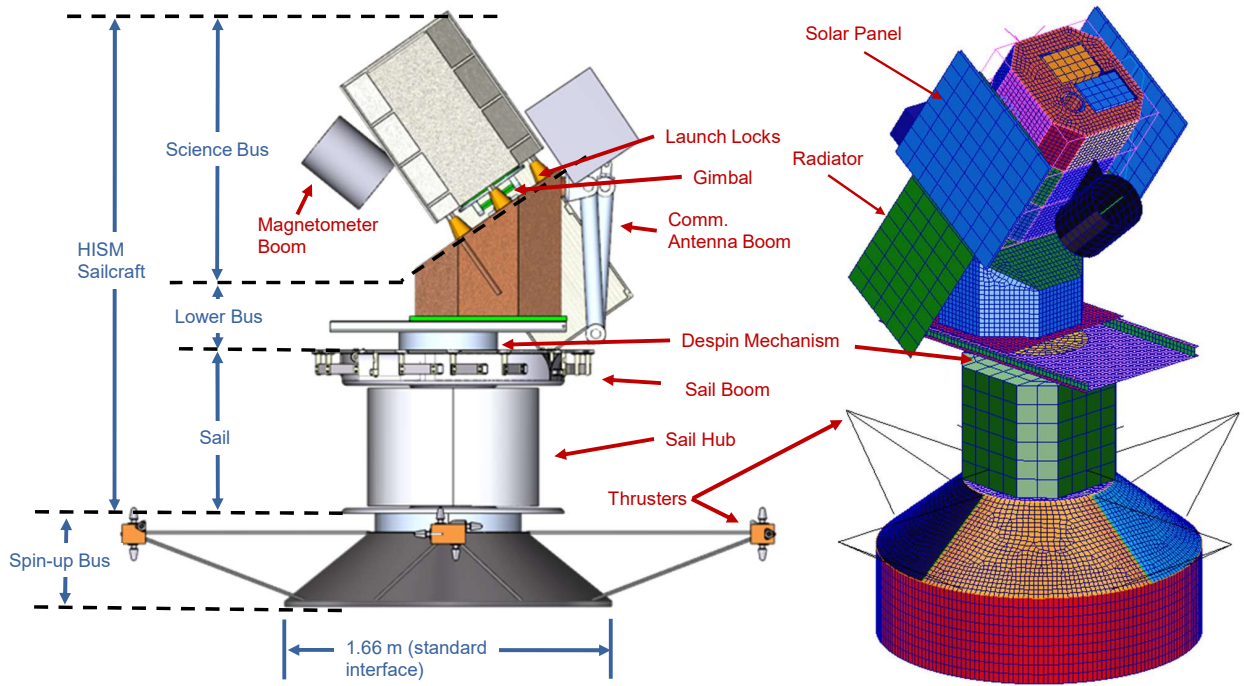


Figure 6: Spacecraft in stowed configuration.

rotary joint, but is allowed to precess with the sail. The Lower Bus contains the sailcraft avionics (section 4.6), solar panel arrays, and the communication antenna boom. The Science Bus contains all the science instruments, including the magnetometer boom, and the science instrument electronics. Each bus section has its own passive cooling system (Section 4.10). The connection between the Science Bus and Lower Bus is through a freely moving gimbal mechanism, with 3 degrees of freedom. Momentum wheels inside the Science Bus keep the science instruments pointed at the Sun to the required pointing accuracy and stability; when the momentum wheels are saturated, the gimbal mechanism is driven to the limit of the motion range to transfer momentum to the sail, to be de-saturated using the RCDs. The Science Bus is mounted at a nominal angle of 35.3° angle relative to the solar sail surface, corresponding to the optimal cone angle during the cranking phase of the mission.

4.3 Spin-up Bus

The Spin-up Bus is a modified launch vehicle adapter and fulfills that function during launch. The bus also contains a propulsion system for initial attitude control and to spin up the sail during sail deployment. After the sail is deployed, the Spin-up Bus is jettisoned. To perform a safe jettison and disposal, the Spin-up Bus contains a simple controller and a bare minimum of navigation sensors (IMU and coarse sun sensor) which control the propulsion system to fly away from the sailcraft. The propulsion system is a blowdown hydrazine monopropellant system with 16 thrusters, each with 4N thrust and arranged into 4 pods of 4 thrusters each

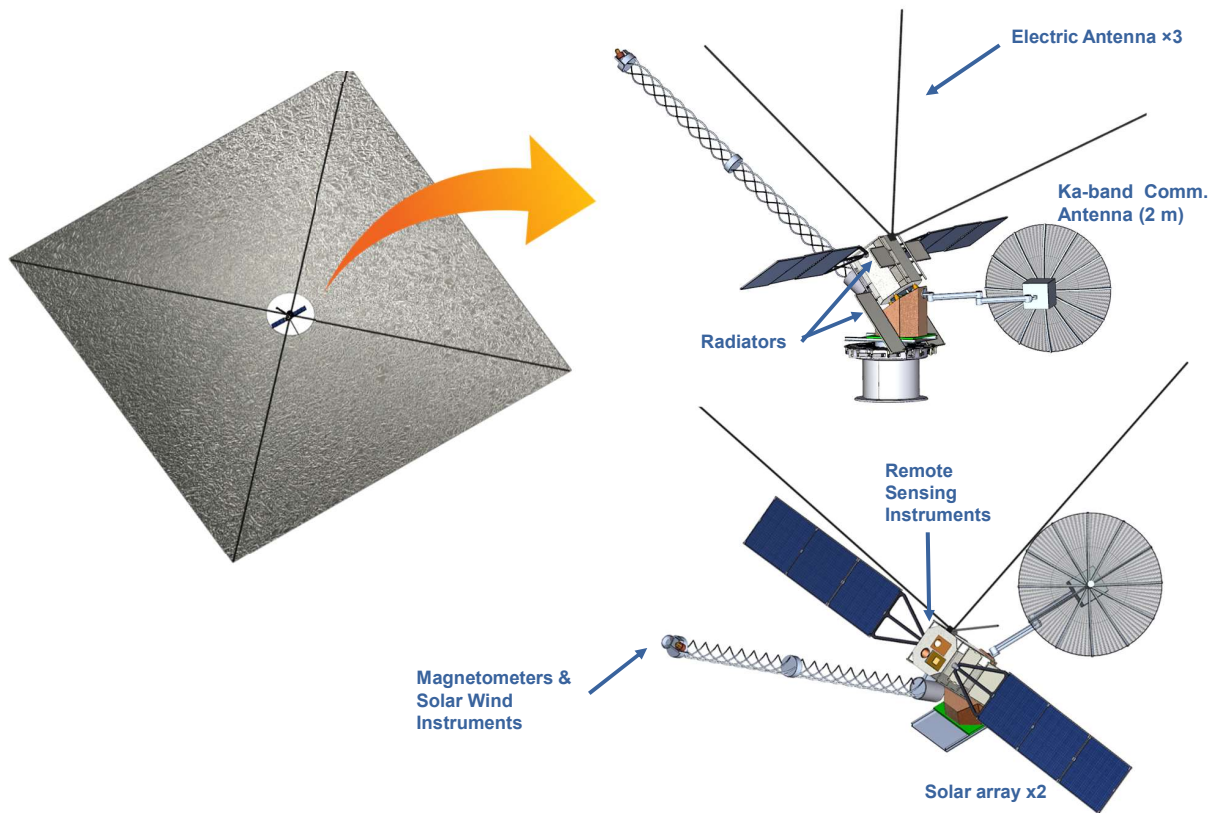


Figure 7: Sailcraft in fully deployed configuration, full sailcraft (left) and bus detail (right). During the cranking phase of the mission, the sail is held at a constant 35.3 degree angle relative to the Sun-spacecraft line. The sailcraft bus is designed with this angular offset, nominally pointing 35.3 degrees from the sail normal. The boom and electrical antennas are angled as far from the sail and from each other as possible. The sail has a 10 m hole in the center, which minimizes its effect on the science instruments and radiative coupling with the sailcraft bus.

and located 1.75 m from the spacecraft centerline.

The total wet mass of the propulsion system is estimated to be 13.1 kg. However, because the Spin-Up Bus is not part of the sailcraft, the system may be replaced with a lower efficiency (higher mass) system, such as cold-gas thrusters, without affecting the sailcraft performance.

4.4 Sail System

The HISM concept is based on the Solar Cruiser mission, currently in Phase A development at MSFC. The sail for the Solar Cruiser mission is 1,666 m² and provides a characteristic acceleration (A_c) of 0.17 mm/s². The sail architecture comprises a four quadrant sail design with four composite booms that are deployed from a central rotating deployment mechanism and sail hub. The sail membrane is the space- and sail-proven aluminized CP1 polyimide substrate successfully flown on NanoSail-D2 and to be flown on NEA Scout[Sobey and Lockett, 2016].

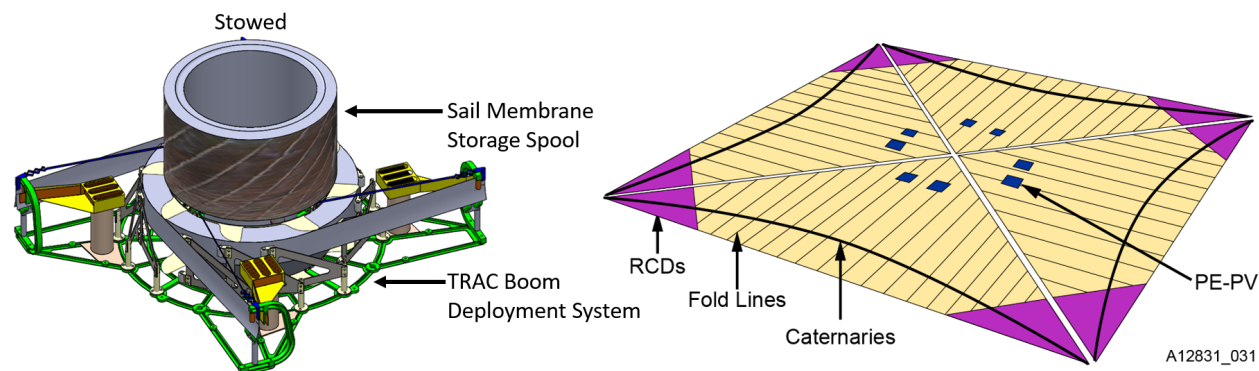


Figure 8: Solar Cruiser Solar Sail Stowed (left) and Deployed (right)

The Solar Cruiser solar sail is pictured in both the stowed and deployed configurations in Figure 8. The solar sail membrane is deployed and tensioned using four Triangular, Rollable, and Collapsible (TRAC) high strain composite (HSC) booms, the same geometry of the boom flight-validated by NanoSail-D2 and used on the upcoming NEA Scout mission. TRAC booms have a triangular cross section that flattens and rolls around a central spool for stowage. Deployment is actuated via a single motor controlled by the bus. This proven design has higher strength/weight for a given flattened height than other rollable boom designs[Banik and Murphey, 2010] is easy to fabricate and taper, and has flight heritage. The double omega boom was rejected due to the manufacturing difficulties for long booms, expensive tooling, space constraints of the stowed system, and the sail application does not require the additional torsional stiffness.

The HISM sail is equipped with Reflectivity Control Devices (RCDs, see section 4.8) for attitude control, along with Polyimide Embedded Photovoltaics (PE-PV) generating power for the RCDs. Both technologies will be demonstrated on the Solar Cruiser, further advancing the solar sail architecture.

Roccor conducted a feasibility study with a tentative goal of scaling the Solar Cruiser sail design to $A_c = 0.3$ mm/s² with a payload (non-sail-subsystem) mass of 140 kg. The sail membrane was assumed to be the same design as Solar Cruiser (2.5 μ m CP1 substrate),

and the sail system configuration was assumed to be the same as well, i.e. 4 sail quadrants supported by 4 tapered composite TRAC booms on a common spool for deployment. For a rigid or non-spinning sail system such as Solar Cruiser, each boom is under compressive stress from sail tension, and therefore the driving constraint for sizing of the system is the buckling of the booms. The tension requirement itself is derived from the stiffness requirement of the deployed system, i.e. maintaining a sufficiently high first mode natural frequency, as well as the flatness requirement of the sail membranes. As sail sizes become very large, the size and mass of the booms required to tension the sail become disproportionately large. The study concluded that, in order to meet the HISM requirements, sail tension would need to be imparted using centrifugal force by spinning the sail at ~ 1 rpm. This centrifugal force reduces the buckling strength requirement of the composite TRAC booms, significantly decreasing their mass. Since the booms are no longer required for sail tension, their primary function then becomes to provide out of plane stiffness to the sail membrane to improve sail-flatness and to reduce attitude control complexities experienced by other spinning sail missions such as IKAROS[Yuki, 2017]. The resulting design achieves a 52 kg sail subsystem mass with a 7000 m² sail area, including 4 booms, sail membranes, stowage spools, deployment mechanism, and 3 kg allowance for RCDs.

4.5 Structures

The HISM structure has been designed to meet strength and stability requirements in NASA-STD 5001B, assuming a Falcon-9 launch vehicle. A conventional all-metal construction using 2000 series aluminum and Hexcel aluminum core is assumed. The structural model is shown in figure 6 (right). The structural mass of the science bus and lower bus are estimated to be 22.2 kg and 23.2 kg respectively.

4.6 Command and Data Handling

The spacecraft avionics performs all command and data handling for the spacecraft, and perform the data storage and downlink operations for the science instruments. It is a 10-board stack of PCI104s form factor avionics boards, consisting of: a Single Board Computer (SBC) for flight control, a digital signal processor board for data management and formatting of instrument data, a digital I/O board and an analog I/O board, three memory storage boards, a reaction wheel controller/driver board, an antenna gimbal controller/driver board, and the avionics stack power supply board. Mass and power estimates are based on currently available components with flight heritage, such as the Space Micro Proton 400k SBC. The memory boards provide 8GBytes each, for a total of 24GBytes of on-board memory storage. The predicted mass of the avionics system is 9.7 kg, including cabling, and power consumption is 84.3 W.

4.7 Communications

The HISM communication system consists of an X-band system with non-directional patch antennas and a Ka-band system using a 2-meter antenna. The X-band system is used

for initial checkout and sail deployment. The Ka-band system is used for all subsequent communications, while the X band system remains available as a backup.

The X-band system consists of a Tether Unlimited SWIFT XTX 7-watt transceiver, 4 patch antennas on the sailcraft bus, and an additional patch antenna on the Spin-up Bus, allowing uninterrupted communications in all directions during sail deployment. During sail deployment, expected to occur at a distance of 400k to 600k km from Earth, the X-band system is capable of 2 Mbps downlink to a DSN 34m antenna with 54 G/T. This allows for 1 fpm uncompressed full-HD video from two onboard cameras, or a higher rate if compression is used.

During the science observing phase (cranking phase) of the mission, science data is generated at an average rate of 275 kbps (Table 1). With 4:1 compression for science data, 2.5 kbps spacecraft telemetry and 30% margin, the data volume is 8.0 Gbits/day. A Ka-band system with a 2-meter antenna 38W RF power has been selected as an optimal balance between DSN cost, RF power and antenna size. This configuration is capable of 1 Mbps downlink at the mission’s maximum Earth-spacecraft distance of 220 Gm, requiring 2.2 hours of downlink time per day at this distance. A General Dynamics (GD) Small Deep-Space Transponder (SDST) and along with Bosch Ka-band AstralK Traveling Wave Tube Amplifier (TWTA) are assumed for this study.

Because the required sail orientation and Sun-pointing science instruments constrain the spacecraft attitude, the Earth can be almost any direction relative to the spacecraft. A 5-meter long articulated, gimballed antenna boom is used to insure communications throughout the mission. A 2-axis gimbal unit is placed at the mount of the antenna to the boom, while the boom its self has 3 axes of movement: two at the boom to S/C union, and one at the boom joint. The antenna boom system is estimated at 11 kg, including 2.5 kg for actuators and 6 kg for the 2-meter mesh antenna itself.

4.8 Guidance, Navigation and Control

The GNC subsystem has some challenges for the HISM mission. The large sail and high spin rate lead to a large amount of angular momentum stored in the sail. This removes traditional attitude control actuators (RCS thrusters or reaction wheels) from the trade space for controlling the sail attitude. To do coarse steering of the vehicle, RCDs and active mass transfer (AMT) were both studied for HISM.

RCDs are liquid-crystal devices that switch between transparent and translucent (diffuse) states based on the applied voltage. This principle has been successfully tested on the IKAROS mission [Funase et al., 2011] and is also currently under development by Nexolve for the Solar Cruiser. A set of 8 RCD panels, each with a 4.6 m² area and located at the outer corners of each sail quadrant, is baselined for the HISM design. This allows for 10°/day slew rate in the 0.48 AU orbit. Following the Solar Cruiser design, the RCDs are placed at an angle relative to the sail plane, allowing for roll torque to be generated by selectively turning on/off the RCDs. Each RCD is powered by sail-embedded PE-PV panels, currently under development at MSFC [Johnson et al., 2017]. The PV cells are located near the RCDs, along with a controller, to minimize cable mass and transmission loss. The controllers are commanded from a wireless transmitter in the sailcraft bus.

The active mass transfer (AMT) device is a 2-axis translation mechanism that shifts the

center of mass (CM) of the sailcraft bus relative to the center of pressure (CP) of the sail, generating a pitch or yaw torque. The baseline HISM design uses only RCDs for control of the sail; however, an AMT can be added if a decrease in RCD area is necessary or for redundancy in the system. A slew rate of $10^\circ/\text{day}$ is well within the capability of an AMT with ± 21.5 cm motion range in each axis.

When the sail is deployed, the lower bus will be de-spun through a motor at the sail/bus interface. For attitude knowledge of the sail, the lower bus contains a coarse sun sensor and a star tracker. The science bus contains a star tracker and a more precise sun sensor for fine pointing and pointing knowledge of the science instruments. Three 0.10 NM reaction wheels are contained in the Science Bus to achieve the science instrument pointing requirements (Table 1), using input from the fine sun sensor. An IMU is also included for more accurate rate measurements.

4.9 Power

The HISM sailcraft is designed for operation from 1 AU to 0.48 AU, with the solar irradiance varying by a factor of 4.3. And while full science operation is not planned till the 0.48 AU orbit, the sailcraft requires significant power for survival heaters at 1 AU, owing to the large radiators necessary for operation at 0.48 AU. As a consequence, the HISM power system is designed to provide a maximum of 700 W at 1 AU and 540 W at 0.48 AU.

The primary solar arrays on HISM are two "reflective" solar panels, with a total area of 1.7 m^2 and coated with a pattern of highly reflective gold coating, covering 60% of the total area. This coating reduces solar input to the panel, allowing them to operate at 0.48 AU and generate 540W. These are supplemented by two conventional solar arrays, with a total area of 2 m^2 , generating 458W at 1 AU. At 0.6 AU distance from the Sun, the conventional arrays will be electrically disconnected from the main arrays. The solar arrays are grouped into two deployable arrays. The total mass of the power system, including the panels, control board, power switch board, and harness, is estimated at 20.7 kg.

The sailcraft does not contain any batteries. The power for initial checkup, attitude control, solar array deployment and thruster operation (including propulsion preparation heating) is supplied by a 205 Whr Li-Ion secondary battery inside the Spin-up Bus, to be discarded after sail deployment.

4.10 Thermal Design

The HISM sail is CP1 film with aluminum coating on the Sun side and black chromium coating on the back side. Black chromium has an emissivity of ~ 0.4 ; the sail membrane temperature is estimated to be 120°C at 0.48 AU from the Sun, well below the CP1's temperature limit of 250°C . A 10 m hole in the center of the sail minimizes radiative coupling between the sail and the sailcraft bus. Black chromium is also electrically conductive, which minimizes electrostatic charging of the sail.

The HISM sailcraft is designed for full science operation at 0.48 AU distance from the Sun. The science bus and lower bus are both enclosed in high-temperature multi-layer insulation (MLI), composed of multiple layers of embossed Double Aluminized Kapton with an outer layer of single aluminized Kapton. Other spacecraft elements, such as radiator panels, high-

gain antenna and Solar sail booms and deployment housing are covered with low-absorptivity white paint. Many smaller spacecraft elements are covered with low-absorptivity white paint, high-temperature MLI or other thermal coatings as necessary.

The Science Bus and Lower Bus are each equipped with a pair of deployable heatpipe radiator panels oriented edge-on to the Sun. Heat from internal components are transported to the radiator panels using a network of heatpipes and heatpipe-embedded cold plates. The mass of these control systems is estimated to be 17.8 kg for the Science Bus and 19.9 kg for the Lower Bus.

Because the passive cooling system is designed for full science operation at 0.48 AU, the bus temperatures will fall below the assumed -20°C survival temperatures early in the mission. Survival heaters are used to keep the internal components above the survival temperatures; a total of 310 W power heater power is required at 1 AU with science instruments turned off.

5 Mission Design

5.1 Mission Profile

HISM is launched on a dedicated launcher. With a launch mass of 358 kg and the requirement to be launched into a $C_3 > 0$ trajectory, many existing launch vehicles are suitable for this mission, such as the Falcon-9 or Atlas-V 401. Shortly after the spacecraft (sailcraft + Spin-up Bus) is separated from the launcher, the thrusters in the Spin-up Bus are used to de-tumble the spacecraft and establish attitude control, and the solar arrays on the Lower Bus are deployed. The sail is then deployed, using the Spin-up Bus thrusters to increase the spin rate of the sail and ensure a sufficient spin rate to maintain the sail's structural integrity. After the sail is fully deployed, the Spin-up Bus disconnects from the sailcraft and uses the thrusters to fly away from the sail. The sailcraft then begins the inward spiral phase of the mission (Section 5.2). The sailcraft remains in the ecliptic plane while it reduces the orbital radius from 1 AU to 0.48 AU.

Once a circular orbit is achieved at 0.48 AU, all science instruments will start continual operations. The sailcraft switches from spiraling to cranking operation, where the sail attitude is optimized for orbital inclination change. The orbit is a constant distance from the Sun, and the sail cone angle will also be held constant; only the sail clock angle (roll angle around the sailcraft-Sun line) will change. From this point on, the sailcraft continues to increase its orbital inclination (Figure 10). There is no defined end to the cranking phase; with no onboard consumables and assuming the sailcraft remains operational, it will eventually reach 90° inclination. At this point the sailcraft may continue cranking past 90° , or allow its orbital inclination to oscillate around 90° .

5.2 Mission Analysis

Minimum time trajectories for the inward spiral phase and cranking phase were generated for various sail characteristic accelerations, A_c , which is a sailcraft performance metric that represent the thrust accelerations that sails can achieve at a solar distance of 1 AU with

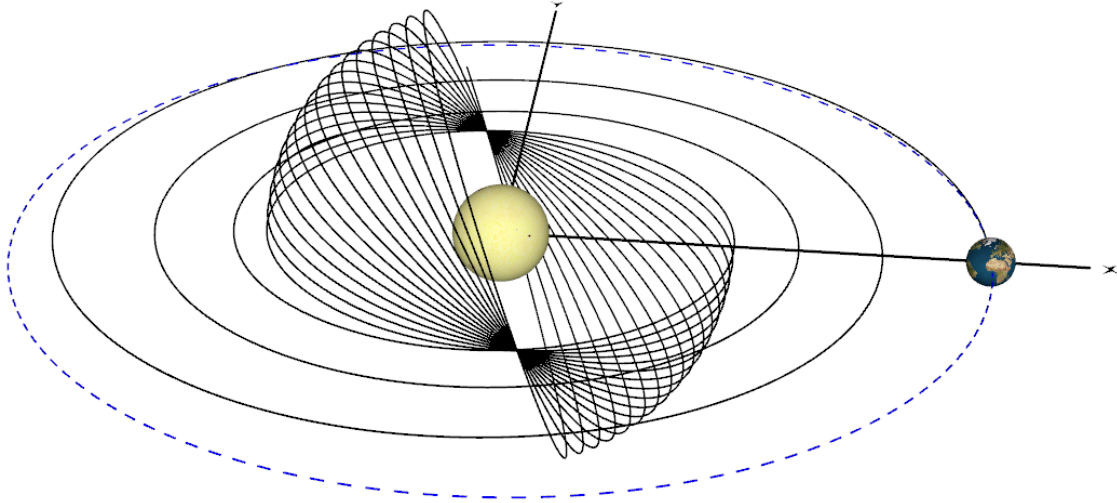


Figure 9: Solar Sail Mission Trajectory from Earth ($C_3 = 0$) to 0.48 AU and 75 deg Inclination for an Example Sail Characteristic Acceleration of 0.30 mm/s^2

the sail perpendicular to sunlight. For each case, the sail departs Earth with a $C_3 = 0$ and performs an inward spiral to the 0.48 AU solar distance. The sail then begins the "cranking" phase of the mission, during which the sail increases the orbital inclination while maintaining a constant distance from the Sun. Figure 9 shows the inward spiral and cranking phases for a sail A_c of 0.3 mm/s^2 .

Trajectories for the spiral and cranking phases were each optimized separately. For the spiral-in phase, a minimum time trajectory was calculated with initial conditions of $C_3 = 0$ (i.e. launched from Earth at escape speed), $r = 1 \text{ AU}$ and $v_r = 0$. The targeted final conditions were $r = 0.48 \text{ AU}$, $v_r = 0$ and $dv_r/dt = 0$. The cone angle (angle between the sail normal and sunlight) was allowed to vary for optimization, while the clock angle was held at 270° . For the cranking phase, the clock angle was held at 270° to maximize the lateral component of thrust. During the cranking phase, the cone angle is held constant at 35.3° , while the clock angle is varied to maintain the constant solar distance. The sun incidence angle is required to change from 35.3° towards ecliptic north to 35.3° towards ecliptic south and vice versa for each orbit. These two maneuvers were assumed to be instantaneous for the purposes of this study.

Minimum time trajectories were generated over a range of characteristic accelerations. Figure 10 shows the orbital parameters throughout the mission; $A_c = 0.22 \text{ mm/s}^2$ and 0.26 mm/s^2 represent characteristic accelerations based on the mass estimates from this study – with and without mass margin, respectively. The $A_c = 0.3 \text{ mm/s}^2$ case is also displayed for comparison purposes. Mission durations are shown in Table 2.

6 Conclusions

A spacecraft in high inclination ($> 60^\circ$) orbit, equipped with a combination of remote sensing and in-situ instrument, has the potential to dramatically change our understanding of the Sun and the heliosphere. The HISM concept study demonstrates the feasibility of such

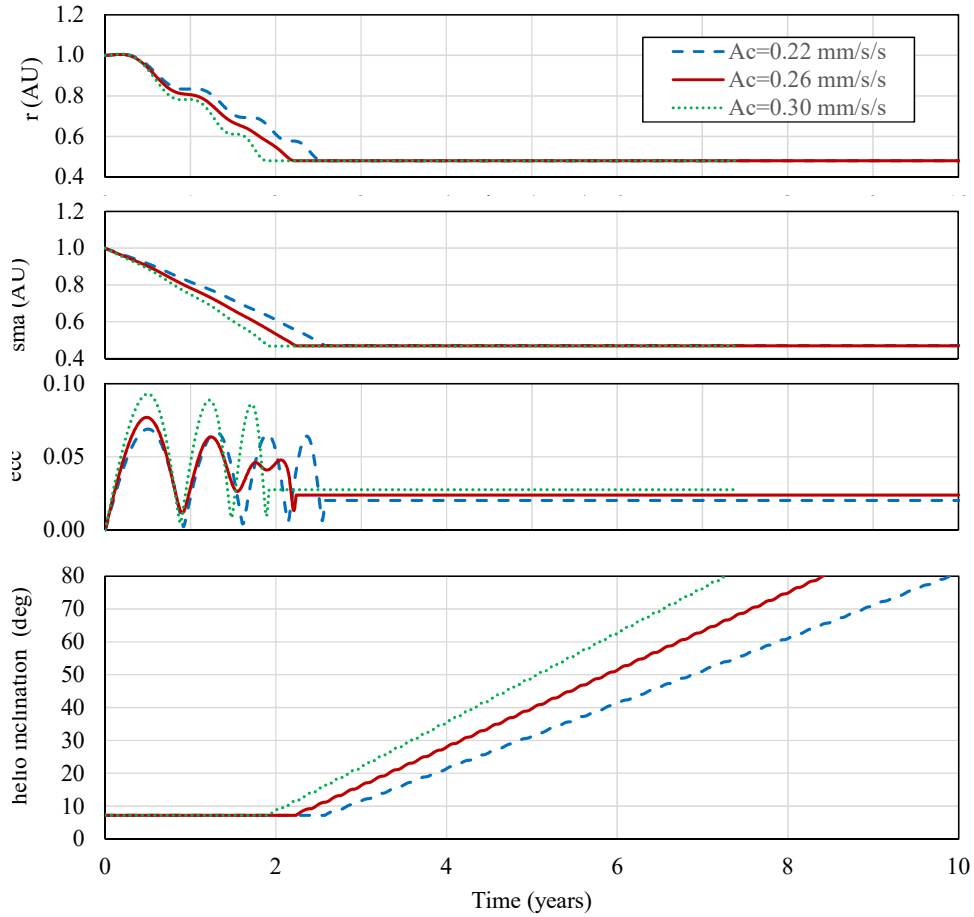


Figure 10: Spacecraft distance from Sun – along with orbital semi-major axis, eccentricity and inclination (relative to the Sun’s equator) – plotted for 3 different characteristic accelerations. $A_C = 0.26 \text{ mm/s}^2$ corresponds to the HISM design and predicted mass (without margin); at this characteristic acceleration, duration from launch to 0.48 AU is 2.2 years. Heliographic inclination of 60° is reached 6.7 years after launch, and 75° at 8.0 years.

Table 2: Times to Key Mission Events for Sailcraft with Characteristic Accelerations of 0.22, 0.26, and 0.30 mm/s². Total times are given to 60° and 75° Heliographic Inclinations

	$A_C = 0.22 \text{ mm/s}^2$	$A_C = 0.26 \text{ mm/s}^2$	$A_C = 0.30 \text{ mm/s}^2$
Time to 0.48 AU [yr]	2.6	2.2	1.9
Total time to 60° [yr]	7.9	6.7	5.8
Total time to 75° [yr]	9.4	8.0	6.9

a mission using currently available components and technologies, and by using the solar sail technology currently under development for Solar Cruiser. The mission accommodates 46 kg of science instrument payload (60 kg including margin), including remote sensing instruments requiring 2 arcminute pointing accuracy and 7 arcsec/second stability. The sailcraft basic mass, estimated based on currently available components, is estimated at 240 kg, achieving a characteristic acceleration of 0.26 mm/s² which is sufficient to reach a 60° inclination (heliographic) in 6.7 years from launch. Because the sailcraft has no onboard consumables, the maximum inclination and mission life are only limited by operations funding and longevity of the sailcraft components. With mass margin, and absent further improvements in available components, the characteristic acceleration is 0.22 mm/s², requiring 7.9 years from launch to 60°.

References

- D. Alexander, A. Sandman, P. Liewer, J. Ayon, B. Goldstein, N. Murphy, M. Velli, L. Floyd, D. Moses, D. Socker, A. Vourlidas, G. Garbe, S. Suess, D. Hassler, A. Kosovichev, R. Mewaldt, M. Neugebauer, R. Ulrich, and T. Zurbuchen. Solar Polar Imager: Observing Solar Activity from a New Perspective. In B. Fleck, T. H. Zurbuchen, and H. Lacoste, editors, *Solar Wind 11/SOHO 16, Connecting Sun and Heliosphere*, volume 592 of *ESA Special Publication*, page 663, Sept. 2005.
- T. Appourchaux, P. Liewer, M. Watt, D. Alexander, V. Andretta, F. Auchère, P. D’Arrigo, J. Ayon, T. Corbard, S. Fineschi, W. Finsterle, L. Floyd, G. Garbe, L. Gizon, D. Hassler, L. Harra, A. Kosovichev, J. Leibacher, M. Leipold, N. Murphy, M. Maksimovic, V. Martinez-Pillet, B. S. A. Matthews, R. Mewaldt, D. Moses, J. Newmark, S. Régnier, W. Schmutz, D. Socker, D. Spadaro, M. Stuttard, C. Trosseille, R. Ulrich, M. Velli, A. Vourlidas, C. R. Wimmer-Schweingruber, and T. Zurbuchen. POLAR investigation of the Sun—POLARIS. *Experimental Astronomy*, 23(3):1079–1117, Mar. 2009. doi: 10.1007/s10686-008-9107-8.
- T. Appourchaux, F. Auchère, E. Antonucci, L. Gizon, M. MacDonald, H. Hara, T. Sekii, D. Moses, and A. Vourlidas. SOLARIS: Solar Sail Investigation of the Sun. *arXiv e-prints*, art. arXiv:1707.08193, July 2017.
- J. Banik and T. Murphey. Performance validation of the triangular rollable and collapsible mast. In *24th Annual AIAA/USU Conference on Small Satellites*, volume 2010, 2010.

- T. E. Berger, N. Bosanac, T. R. Smith, N. A. Duncan, G. Wu, E. Turner, N. Hurlburt, and C. Korendyke. The Solar Polar Observing Constellation (SPOC) Mission: research and operational monitoring of space weather from polar heliocentric orbits. In *AGU Fall Meeting Abstracts*, volume 2019, pages SH43F–3352, Dec. 2019.
- B. de Pontieu, S. McIntosh, V. H. Hansteen, M. Carlsson, C. J. Schrijver, T. D. Tarbell, A. M. Title, R. A. Shine, Y. Suematsu, S. Tsuneta, Y. Katsukawa, K. Ichimoto, T. Shimizu, and S. Nagata. A Tale of Two Spicules: The Impact of Spicules on the Magnetic Chromosphere. *Pub. Astron. Soc. Japan*, 59:S655, Nov. 2007. doi: 10.1093/pasj/59.sp3.S655.
- B. De Pontieu, S. W. McIntosh, M. Carlsson, V. H. Hansteen, T. D. Tarbell, C. J. Schrijver, A. M. Title, R. A. Shine, S. Tsuneta, Y. Katsukawa, K. Ichimoto, Y. Suematsu, T. Shimizu, and S. Nagata. Chromospheric Alfvénic Waves Strong Enough to Power the Solar Wind. *Science*, 318(5856):1574, Dec. 2007. doi: 10.1126/science.1151747.
- M. Dikpati and S. W. McIntosh. Space Weather Challenge and Forecasting Implications of Rossby Waves. *Space Weather*, 18(3):e02109, Mar. 2020. doi: 10.1029/2019SW002109.
- L. A. Fisk and J. C. Kasper. Global Circulation of the Open Magnetic Flux of the Sun. *Astrophys. J. Lett.*, 894(1):L4, May 2020. doi: 10.3847/2041-8213/ab8acd.
- L. A. Fisk, T. H. Zurbuchen, and N. A. Schwadron. On the Coronal Magnetic Field: Consequences of Large-Scale Motions. *Astrophys. J.*, 521(2):868–877, Aug. 1999. doi: 10.1086/307556.
- R. Funase, Y. Shirasawa, Y. Mimasu, O. Mori, Y. Tsuda, T. Saiki, and J. Kawaguchi. Fuel-free and Oscillation-free Attitude Control of IKAROS Solar Sail Spacecraft Using Reflectivity Control Device. *Proceedings of the 28th International Symposium on Space Technology and Science*, 2011.
- D. M. Hassler, I. E. Dammasch, P. Lemaire, P. Brekke, W. Curdt, H. E. Mason, J.-C. Vial, and K. Wilhelm. Solar Wind Outflow and the Chromospheric Magnetic Network. *Science*, 283:810, Feb. 1999. doi: 10.1126/science.283.5403.810.
- R. Howard and B. J. Labonte. The sun is observed to be a torsional oscillator with a period of 11 years. *Astrophys. J. Lett.*, 239:L33–L36, July 1980. doi: 10.1086/183286.
- R. Howe, J. Christensen-Dalsgaard, F. Hill, R. W. Komm, R. M. Larsen, J. Schou, M. J. Thompson, and J. Toomre. Dynamic Variations at the Base of the Solar Convection Zone. *Science*, 287(5462):2456–2460, Mar. 2000. doi: 10.1126/science.287.5462.2456.
- L. Johnson, J. Carr, and D. Boyd. The Lightweight Integrated Solar Array and anTenna (LISAT) Big Power for Small Spacecraft,. *68th International Astronautical Congress (IAC)*, 2017.
- P. C. Liewer. Solar Polar Imager: Observing Coronal Transients from a New Perspective (Invited). In *AGU Fall Meeting Abstracts*, volume 2013, pages SH51D–02, Dec. 2013.

- P. C. Liewer, J. Ayon, D. Alexander, A. Kosovichev, R. A. Mewaldt, D. G. Socker, and A. Vourlidas. Solar Polar Imager: Observing Solar Activity from a New Perspective. In M. S. Allen, editor, *NASA Space Science Vision Missions*, volume 224, page 1, 2008.
- E. Marsch, R. Marsden, R. Harrison, R. Wimmer-Schweingruber, and B. Fleck. Solar Orbiter—mission profile, main goals and present status. *Advances in Space Research*, 36(8): 1360–1366, Jan. 2005. doi: 10.1016/j.asr.2004.11.012.
- D. J. McComas, B. L. Barraclough, H. O. Funsten, J. T. Gosling, E. Santiago-Muñoz, R. M. Skoug, B. E. Goldstein, M. Neugebauer, P. Riley, and A. Balogh. Solar wind observations over Ulysses’ first full polar orbit. *J. Geophys. Res.*, 105(A5):10419–10434, May 2000. doi: 10.1029/1999JA000383.
- S. W. McIntosh. Recent Observations of Plasma and Alfvénic Wave Energy Injection at the Base of the Fast Solar Wind. *Space Sci. Rev.*, 172(1-4):69–87, Nov. 2012. doi: 10.1007/s11214-012-9889-x.
- S. W. McIntosh, R. J. Leamon, and B. De Pontieu. The Spectroscopic Footprint of the Fast Solar Wind. *Astrophys. J.*, 727(1):7, Jan. 2011. doi: 10.1088/0004-637X/727/1/7.
- S. W. McIntosh, X. Wang, R. J. Leamon, A. R. Davey, R. Howe, L. D. Krista, A. V. Malanushenko, R. S. Markel, J. W. Cirtain, J. B. Gurman, W. D. Pesnell, and M. J. Thompson. Deciphering Solar Magnetic Activity. I. On the Relationship between the Sunspot Cycle and the Evolution of Small Magnetic Features. *Astrophys. J.*, 792(1):12, Sept. 2014. doi: 10.1088/0004-637X/792/1/12.
- S. W. McIntosh, R. J. Leamon, L. D. Krista, A. M. Title, H. S. Hudson, P. Riley, J. W. Harder, G. Kopp, M. Snow, T. N. Woods, J. C. Kasper, M. L. Stevens, and R. K. Ulrich. The solar magnetic activity band interaction and instabilities that shape quasi-periodic variability. *Nature Communications*, 6:6491, Apr. 2015. doi: 10.1038/ncomms7491.
- S. W. McIntosh, W. J. Cramer, M. Pichardo Marcano, and R. J. Leamon. The detection of Rossby-like waves on the Sun. *Nature Astronomy*, 1:0086, Mar. 2017. doi: 10.1038/s41550-017-0086.
- S. W. McIntosh, R. J. Leamon, R. Egeland, M. Dikpati, Y. Fan, and M. Rempel. What the Sudden Death of Solar Cycles Can Tell Us About the Nature of the Solar Interior. *Solar Phys.*, 294(7):88, July 2019. doi: 10.1007/s11207-019-1474-y.
- National Research Council. *Solar and Space Physics: A Science for a Technological Society*. The National Academies Press, Washington, DC, 2013. ISBN 978-0-309-16428-3. doi: 10.17226/13060. URL <https://www.nap.edu/catalog/13060>.
- R. Ridenoure, R. Munakata, A. Diaz, S. Wong, B. Plante, D. Stetson, D. Spencer, and J. Foley. LightSail Program Status: One Down, One to Go,. *Proceedings of the 29th Annual AIAA/USU Conference on Small Satellites*, 2015.

- T. Russell-Lockett, J. Castillo-Rogez, L. Johnson, J. Matus, J. Lightholder, and A. Marian. Near-Earth Asteroid Scout Flight Mission. *IEEE Aerospace and Electronic Systems Magazine*, 35(3), 2020.
- H. B. Snodgrass and P. R. Wilson. Solar torsional oscillations as a signature of giant cells. *Nature*, 328(6132):696–699, Aug. 1987. doi: 10.1038/328696a0.
- A. Sobey and T. Lockett. Design and development of nea scout solar sail deployer mechanism. In *43rd Aerospace Mechanisms Symposium*, volume 2016, 2016.
- M. J. Thompson, J. Toomre, E. R. Anderson, H. M. Antia, G. Berthomieu, D. Burtonclay, S. M. Chitre, J. Christensen-Dalsgaard, T. Corbard, M. De Rosa, C. R. Genovese, D. O. Gough, D. A. Haber, J. W. Harvey, F. Hill, R. Howe, S. G. Korzennik, A. G. Kosovichev, J. W. Leibacher, F. P. Pijpers, J. Provost, J. Rhodes, E. J., J. Schou, T. Sekii, P. B. Stark, and P. R. Wilson. Differential Rotation and Dynamics of the Solar Interior. *Science*, 272(5266):1300–1305, May 1996. doi: 10.1126/science.272.5266.1300.
- S. Tomczyk, S. W. McIntosh, S. L. Keil, P. G. Judge, T. Schad, D. H. Seeley, and J. Edmondson. Alfvén Waves in the Solar Corona. *Science*, 317(5842):1192, Aug. 2007. doi: 10.1126/science.1143304.
- A. Vourlidas, P. C. Liewer, M. Velli, and D. Webb. Solar Polar Diamond Explorer (SPDEx): Understanding the Origins of Solar Activity Using a New Perspective. *arXiv e-prints*, art. arXiv:1805.04172, May 2018.
- K. P. Wenzel, R. G. Marsden, D. E. Page, and E. J. Smith. The ULYSSES Mission. *Astron. Astrophys. Suppl.*, 92:207, Jan. 1992.
- P. R. Wilson, R. C. Altrock, K. L. Harvey, S. F. Martin, and H. B. Snodgrass. The extended solar activity cycle. *Nature*, 333(6175):748–750, June 1988. doi: 10.1038/333748a0.
- T. Yamaguchi, Y. Mimasu, Y. Tsuda, R. Funase, H. Sawada, O. Mori, M. Morimoto, H. Takeuchi, and M. Yoshikawa. Trajectory analysis of small solar sail demonstration spacecraft ikaros considering the uncertainty of solar radiation pressure. *Transactions of the Japanese Society for Artificial Intelligence, Aerospace Technology Japan*, 8(ists27): 37–32, 2010.
- T. Yuki. Attitude and orbit control of a spinning solar sail by the vibrational input on the sail membrane. In *International Symposium on Space Flight Dynamics*, volume 2017, 2017.